Turkish Journal of Electrical Engineering & Computer Sciences

http://journals.tubitak.gov.tr/elektrik/

Research Article

Turk J Elec Eng & Comp Sci
(2015) 23: 1660 – 1672

doi:10.3906/elk-1404-191

Performance improvement of three-phase self-excited induction generator feeding induction motor load

Jyotirmayee DALEI*, Kanungo Barada MOHANTY
Department of Electrical Engineering, National Institute of Technology, Rourkela, India

Received: 11.04.2014 • **Accepted/Published Online:** 11.02.2015 • **Printed:** 30.11.2015

Abstract: In this paper, the transient and steady-state performances of an isolated self-excited induction generator driven by a wind turbine and feeding power to a dynamic load such as a three-phase induction motor are analyzed. Mathematical modeling and simulation study of the whole system, including the wind turbine, induction generator, capacitor, pulse width modulated voltage source inverter, and dynamic load, are carried out with closed-loop voltage and frequency controller. The complete system is modeled in the stationary $d-q$ frame and validated by comparing simulation and experimental results at no-load. The same mathematical model is then used to study the transient performance of the self-excited induction generator supplying to a dynamic load. When the induction motor is connected to the induction generator without any voltage and frequency controller, it causes severe transients in electrical and mechanical variables of the generator. Due to the large starting-current requirement of the induction motor, there is a collapse of the terminal voltage of the generator. A bidirectional pulse width modulated source inverter with DC link battery is connected with the generator and operated in closed-loop control mode to maintain voltage and frequency and to operate the induction motor successfully with variable wind speed and mechanical load.

Key words: Wind turbine, self-excited induction generator, dynamic modeling, pulse width modulated voltage source inverter, PI controller

1. Introduction

Renewable energy sources, such as wind, photovoltaic, and hydropower plants are recently being paid much attention universally due to excess exploitation of fossil fuels and associated environment pollution. The self-excited induction generator (SEIG) is suitable to generate electrical power from these nonconventional energy sources [1, 2, 3].

To operate as a self-excited induction generator, an induction machine has to be provided with magnetizing energy. This can be achieved by connecting the capacitor bank [4] across the stator terminals. The major problems with the SEIG are as follows: its terminal voltage and frequency are influenced by the prime mover speed, excitation capacitance, load current, and power factor of the load.

With a fixed capacitor bank connected across the stator terminals, it is not possible to keep the terminal voltage of the SEIG constant under varying loads because of the variable reactive power demand, which is not met by the fixed capacitor bank. Therefore, the major problems associated with SEIG are its poor voltage and frequency regulation. However, due to fast response, improved switching features, and the low cost of the power converters, researchers are attracted to explore their applications for performance improvement of SEIGs

*Correspondence: jyoti_uce@yahoo.com

[5–10]. Wind energy is plentifully available in remote areas, where power grids are not available. Local small-scale standalone systems can utilize these resources where a grid connection is not feasible. In remote areas, the majority of electrical loads are induction motors used for domestic and agricultural purposes to pump water and in flour mills. Therefore, it is vital to study the behavior of the SEIG when it feeds induction motors in standalone applications. Very few research papers have been reported regarding the operation of SEIGs feeding induction motor loads.

Short-shunt and long-shunt schemes were reported in [11], but the schemes involve an iterative method to select the series capacitance. When this type of compensated scheme is used for feeding induction motor load, oscillations and high transients are observed. The dynamic performance of SEIGs feeding induction motor loads was reported in [12], where the damping resistor was connected across series capacitors to damp out the starting transients created by the induction motor when connected to the SEIG and also for getting stable operation. However, this involves complex mathematical calculations for finding the exact value of the damping resistor to be connected across the series capacitor. If the value of damping resistance is low, the system becomes underdamped and voltage collapse occurs. Higher damping resistance makes the system overdamped and oscillations are sustained. Due to damping resistance, additional losses occur. Transient performance of a series-compensated SEIG feeding an induction motor was reported in [13]. For successful operation of the induction motor, proper selection of series and shunt capacitors is required. Otherwise, subsynchronous resonance results. In [14], performance of a SEIG with static synchronous series compensator (SSSC) and static compensator (STATCOM) feeding a dynamic load was reported. The SEIG-SSSC system consists of a unity ratio voltage insertion transformer along with an L-C filter, used to remove high-frequency components from the output voltage of VSC, and two P-I controllers. For generating reference supply current both in-phase current templates and the quadrature current templates are involved in both cases. In [15], a simple scheme was reported with a pulse width modulated (PWM) voltage source inverter (VSI) by taking the R and $R-L$ load only.

Taking these factors into account, this paper focuses on a simple and reliable voltage and frequency controller giving very less transient oscillation and very low THD values for a SEIG-fed induction motor load. In this paper, simulation and experiments on a SEIG with PWM-based VSI feeding induction motor load have been carried out. With the designed control scheme, the VSI is taking care of the induction motor load and source perturbations by injecting the required amount of reactive or active power for maintaining the rated voltage and frequency of the SEIG.

2. System description

The schematic diagram of the whole system is represented in Figure 1. The system consists of a wind turbine, induction machine as SEIG, capacitor bank as excitation system, induction motor as dynamic load, and a PWM VSI. The wind turbine drives the SEIG at a desired speed and appropriate values of capacitor bank are connected across the stator terminals of the SEIG to initiate the self-excitation process and to generate the rated voltage at no-load. Even after the rated voltage is developed, if an induction motor is connected across the SEIG terminals without any controller, terminal voltage across the SEIG collapses. To start and run the induction motor safely, the SEIG is connected with a PWM bidirectional VSI through a coupling transformer and operated in closed-loop control mode.

3. System modeling

The whole system under study has the following components: wind turbine, induction generator, shunt excitation capacitor bank, induction motor load, and PWM VSI.

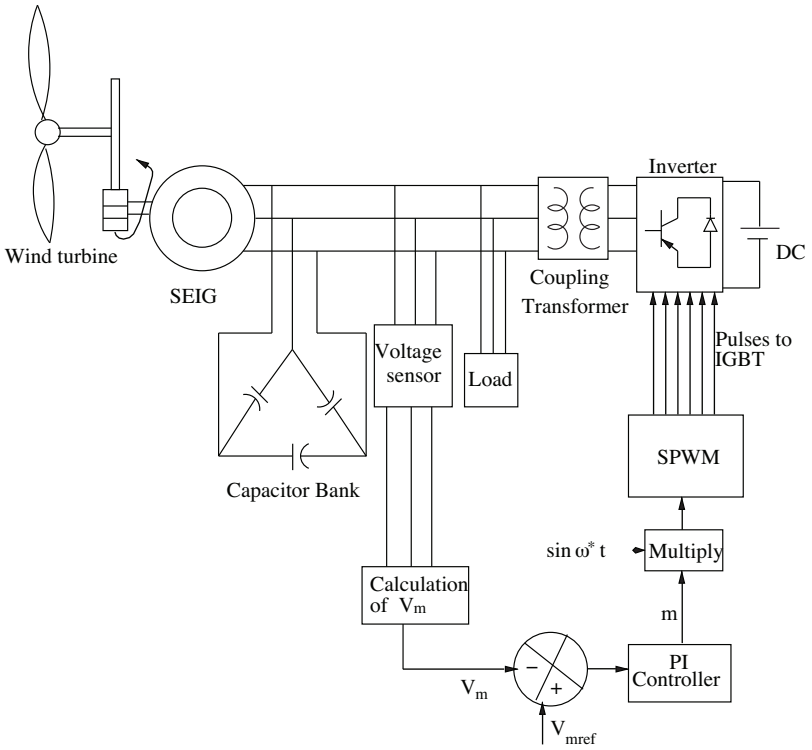

Figure 1. Schematic diagram of SEIG driven by wind turbine with PWM VSI.

3.1. Modeling of wind turbine

The mechanical power P_t captured by a wind turbine [6] of blade radius r running in a wind stream of velocity v_w is given as

$$P_t = 0.5\rho\pi r^2 C_p v_w^3. \tag{1}$$

The tip speed ratio (λ) of the wind turbine can be expressed as

$$\lambda = \frac{w_T r}{v_w}. \tag{2}$$

The polynomial relation between power coefficient C_P and tip speed ratio λ at a particular pitch angle β for the selected wind turbine [6] is

$$C_P(\lambda,\beta) = C_1\left(\frac{C_2}{\lambda_i} - C_3\beta - C_4\right)e^{\left(-\frac{C_5}{\lambda_i}\right)} + C_6\lambda, \tag{3}$$

with $\frac{1}{\lambda_i} = \frac{1}{\lambda+0.08\beta} - \frac{0.035}{\beta^3+1}$ and $C_1 = 0.5176, C_2 = 116, C_3 = 0.4, C_4 = 5, C_5 = 21$, and $C_6 = 0.0068$. The curve between C_P and λ at a zero degree pitch angle is determined as shown in Figure 2, which shows that C_P reaches a maximum value of 0.48 for a maximum tip speed ratio of 8.1, which in turn produces the maximum mechanical power available in the wind turbine for a given wind speed. In fact, the steady-state turbine speed is determined by the power balance [5] at the wind turbine.

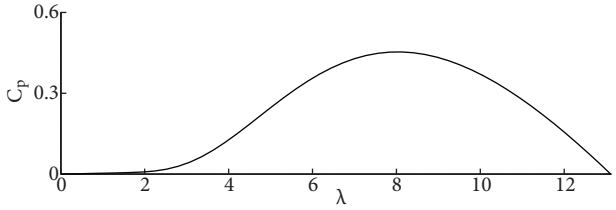

Figure 2. Power coefficient vs. tip speed ratio characteristics of wind turbine.

3.2. Modeling of self-excited induction generator

For the simulation of SEIG in MATLAB/Simulink, the $d-q$ axis stationary frame model of the induction machine [16] is used. Using the $d-q$ component of the stator and rotor currents i_{sd}, i_{sq}, i_{rd}, and i_{rq} as state variables, electrical dynamics of the SEIG are represented through fourth-order state-space model and given by:

$$\frac{di_{sd}}{dt} = \frac{1}{(L_sL_r - L_m^2)}[\omega_r L_m^2 i_{sq} - L_r r_s i_{sd} + \omega_r L_m L_r i_{rq} + L_m r_r i_{rd} + L_r v_{sd}], \tag{4}$$

$$\frac{di_{sq}}{dt} = \frac{1}{(L_sL_r - L_m^2)}[-L_s r_s i_{sq} - \omega_r L_m^2 i_{sd} + L_m r_r i_{rq} - \omega_r L_m L_r i_{rd} + L_r v_{sq}], \tag{5}$$

$$\frac{di_{rd}}{dt} = \frac{1}{(L_sL_r - L_m^2)}[\omega_r L_m L_s i_{sq} + r_s L_m i_{sd} - \omega_r L_s L_r i_{rq} - r_r L_s i_{rd} + L_m v_{sd}], \tag{6}$$

$$\frac{di_{rq}}{dt} = \frac{1}{(L_sL_r - L_m^2)}[r_s L_m i_{sq} + \omega_r L_m L_s i_{sd} - L_s r_r i_{rq} + \omega_r L_s L_r i_{rd} - L_m v_{sq}], \tag{7}$$

where $L_s = L_{ls} + L_m$ and $L_r = L_{lr} + L_m$. Magnetizing current i_m is determined from i_{sd}, i_{sq}, i_{rd}, and i_{rq} using the following expression:

$$i_m = \sqrt{(i_{sd} + i_{rd})^2 + (i_{sq} + i_{rq})^2}. \tag{8}$$

The magnetization characteristic of the SEIG is nonlinear. From synchronous speed tests, the relation between magnetizing inductance L_m and magnetizing current i_m is obtained. A 12th-degree polynomial is considered in [17] for getting good agreement between calculated and measured inductance, but a 5th-degree polynomial is sufficient and was used in [18]. The same polynomial is taken in this paper and given as:

$$L_m = a_5 i_m^5 + a_4 i_m^4 + a_3 i_m^3 + a_2 i_m^2 + a_1 i_m + a_0, \tag{9}$$

where $a_5, a_4, \ldots\ldots$ and a_0 are constants obtained through curve fitting of experimentally obtained characteristics given in Figure 3. The value of these constants are given in the Appendix. The electromagnetic torque T_e of the SEIG is

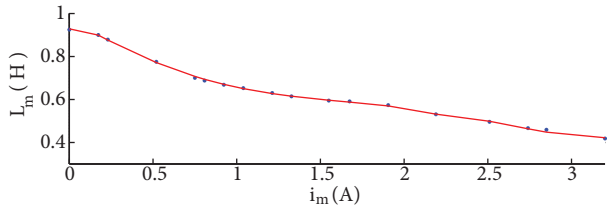

Figure 3. Graph of the identified (blue) and approximated (red) magnetizing inductances vs. magnetizing current.

$$T_e = \left(\frac{3}{2}\right)\left(\frac{P}{2}\right) L_m[i_{sq}i_{rd} - i_{sd}i_{rq}]. \tag{10}$$

The torque balance equation of the SEIG is

$$T_{drive} = T_e + J\left(\frac{2}{P}\right)\frac{d\omega_r}{dt}. \tag{11}$$

The torque balance gives the speed dynamic equation:

$$\frac{d\omega_r}{dt} = \frac{P}{2J}(T_{drive} - T_e). \tag{12}$$

The wind turbine and SEIG are coupled through a gear box and the value of the gear box ratio is given in the Appendix.

3.3. Excitation modeling

The excitation system dynamics are introduced using $d-q$ components of stator voltage (v_{sd} and v_{sq}) as state variables, given as

$$\frac{dv_{sd}}{dt} = \frac{i_{ed}}{C_{ed}}, \tag{13}$$

$$\frac{dv_{sq}}{dt} = \frac{i_{eq}}{C_{eq}}. \tag{14}$$

Three-phase SEIG voltage and current are obtained from $d-q$ to abc values in the stationary reference frame [16], using the following expression.

$$\begin{bmatrix} v_a \\ v_b \\ v_c \end{bmatrix} = \begin{bmatrix} 0 & 1 \\ -\frac{\sqrt{3}}{2} & -\frac{1}{2} \\ \frac{\sqrt{3}}{2} & -\frac{1}{2} \end{bmatrix} \begin{bmatrix} v_{sd} \\ v_{sq} \end{bmatrix} \tag{15}$$

3.4. Modeling of induction motor as dynamic load

The model of the three-phase squirrel cage induction motor used as a dynamic load in the state-space form and in $d-q$ stationary reference frame [19] is given by

$$\frac{d}{dt}[i_m] = [L_m]^{-1}([v_m] - [r_m][i_m] - \omega_{rm}[G_m][i_m]), \tag{16}$$

where $[v_m], [i_m], [r_m], [L_m]$, and $[G_m]$ are defined in the Appendix. The developed electromagnetic torque and torque balance equations [19] are given as

$$T_{eM} = \left(\frac{3P_M}{4}\right)(L_{mM})(i_{sqm}i_{rdm} - i_{sdm}i_{rqm}), \tag{17}$$

$$T_{eM} = T_L + J_M\frac{d\omega_{rM}}{dt}, \tag{18}$$

$$\frac{d\omega_{rM}}{dt} = \frac{P_m}{2J_m}(T_{em} - T_L). \tag{19}$$

3.5. Modeling of PWM three-phase inverter

The output voltage of the inverter [15] is expressed as follows.

$$\begin{bmatrix} v_{invan} \\ v_{invbn} \\ v_{invcn} \end{bmatrix} = \frac{V_{dc}}{3} \begin{bmatrix} 2 & -1 & -1 \\ -1 & 2 & -1 \\ -1 & -1 & 2 \end{bmatrix} \begin{bmatrix} S_a \\ S_b \\ S_c \end{bmatrix} \tag{20}$$

Here, v_{invan}, v_{invbn}, and v_{invcn} are the instantaneous output voltage per phase of the inverter and V_{dc} is the DC voltage in volts. The instantaneous value of current [15] injected into the PCC by the VSI is given as follows.

$$\begin{bmatrix} \frac{di_{inva}}{dt} \\ \frac{di_{invb}}{dt} \\ \frac{di_{invc}}{dt} \end{bmatrix} = \frac{R_s}{L_s} \begin{bmatrix} -1 & 0 & 0 \\ 0 & -1 & 0 \\ 0 & 0 & -1 \end{bmatrix} \begin{bmatrix} i_{inva} \\ i_{invb} \\ i_{invc} \end{bmatrix} + \frac{1}{L_s} \begin{bmatrix} v_a - v_{invan} \\ v_b - v_{invbn} \\ v_c - v_{invcn} \end{bmatrix} \tag{21}$$

Here, R_s and L_s are the resistance and inductance of the coupling transformer.

4. Control scheme

The control scheme is shown in Figure 1. The main objective here is to maintain voltage and frequency of the SEIG constant with the induction motor as a dynamic load and with varying wind speed. The reference and the actual peak voltage per phase are the input variables for the controller, whereas the modulation index is the output variable. A PI controller is considered for maintaining voltage. The PI controller is described by

$$y(t) = K_p \epsilon(t) + K_i \int_0^t \epsilon(t) dt, \tag{22}$$

where $y(t)$ is the output control signal and $\epsilon(t)$ is the input error signal. Here $\epsilon(t) = V_{mref}(t) - V_m(t)$ and $y(t) = m$. V_m is the peak voltage of SEIG phase voltage and is calculated using the following expression.

$$V_m = \sqrt{\frac{2}{3}(v_a^2 + v_b^2 + v_c^2)} \tag{23}$$

K_p and K_i denote the optimized proportional gain and integral gain of the PI controller. The output of the PI controller is responsible for maintaining the terminal voltage of the SEIG. This output is multiplied by the unit sine wave of reference frequency and then compared with the carrier wave to obtain switching functions S_a, S_b, and S_c of the VSI for providing gate signals to the IGBT. For frequency regulation, no extra closed loop is involved in this configuration. When the prime mover speed varies and variable mechanical load is applied to induction motor, this configuration takes care automatically by changing modulation index (m).

The proposed system is modeled and simulcasted using MATLAB/Simulink in order to study its dynamic performance, as described in the next section.

5. Simulation and experimental results

In the laboratory, a 3.7-kW squirrel cage induction machine (SEIG) is coupled to a separately excited DC motor, operated as the prime mover. The parameters of the induction machine are measured experimentally through

DC resistance tests and blocked-rotor tests. The variation of magnetizing reactance is taken into account as it is an important factor for building up voltage and stabilization of the generated voltage.
Figure 3 shows the relation between L_m and i_m obtained from the data measured in the synchronous speed test. Figure 4 shows the experimental setup, which consists of a DC motor used as a prime mover, three-phase squirrel cage induction machine used as SEIG, and fixed capacitor bank.

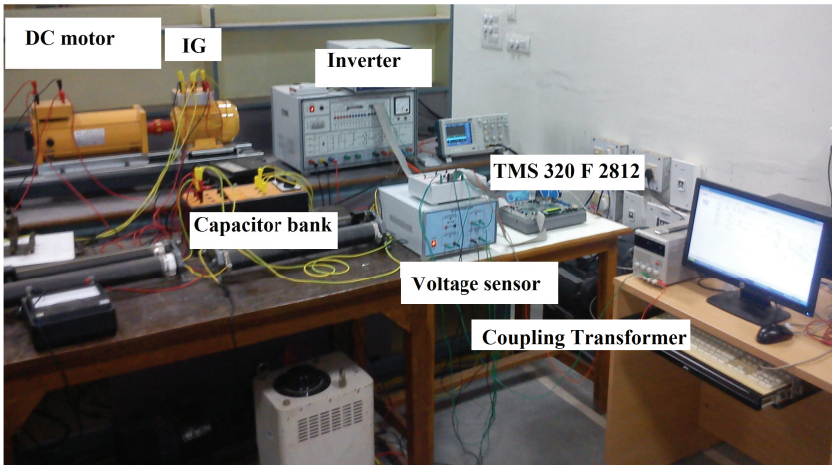

Figure 4. Experimental setup of DC motor coupled induction machine (SEIG) with capacitor bank.

5.1. Voltage buildup at no-load

The capacitor taken both for simulations and experiments is 21 μF per phase at no-load to develop rated SEIG voltage of 415 V (r.m.s.) of a 3.7-kW induction generator. This capacitance is more than the minimum excitation capacitor required, which is calculated using the method given in [18]. Simulation results of voltage build-up process at no-load and corresponding instantaneous stator line current (equal to shunt capacitance currents) are shown in Figures 5a and 5b, respectively. Figure 6 shows the experimental no-load voltage build-up and corresponding current build-up of the same machine taken for simulation; the parameters of the machine are given in the Appendix.

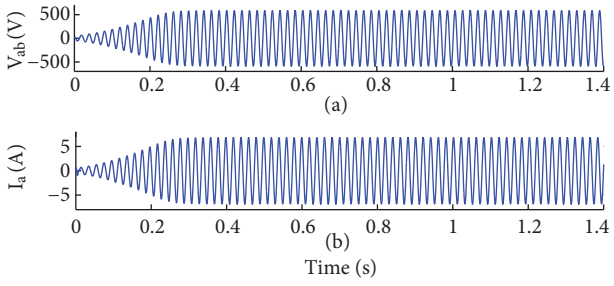

Figure 5. Simulation results of voltage build-up in SEIG at no-load: (a) stator line voltage, (b) stator line current.

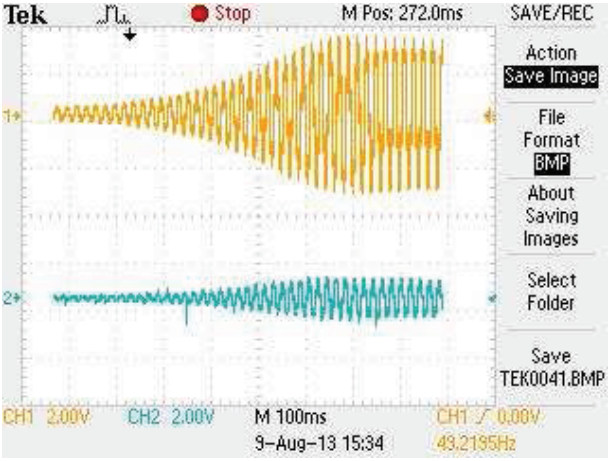

Figure 6. Experimental results of stator voltage build-up of SEIG at no-load (top) and stator line current (bottom).

5.2. Starting transient behavior of SEIG-fed induction motor without any controller

Figure 7 shows the simulation results for voltages and currents of the SEIG feeding an induction motor without any compensator. Figures 7a and 7b show the voltage and current waveforms of the SEIG when the induction motor is directly switched at t = 1.4 s across the stator terminals of the SEIG. It is observed that voltage across the stator terminal of the SEIG collapses and the induction motor fails to run successfully. The corresponding instantaneous line current and speed waveforms of the induction motor are shown in Figures 7c and 7d, respectively.

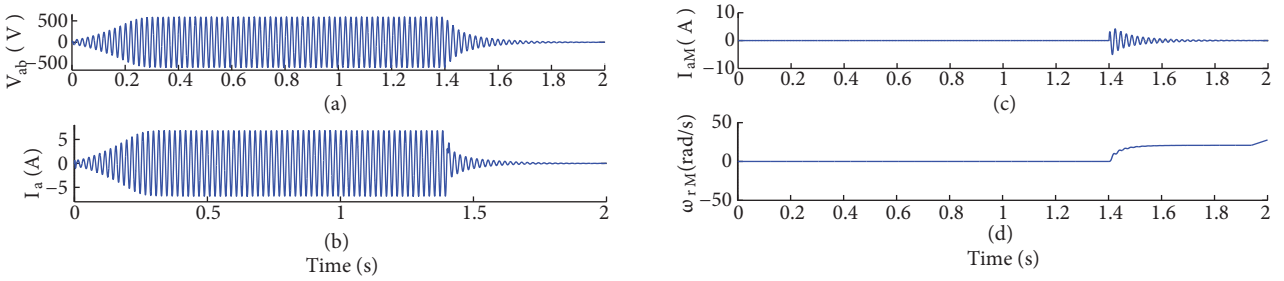

Figure 7. Simulation results of SEIG feeding induction motor directly without any controller: (a) stator line voltage of SEIG, (b) stator line current of SEIG, (c) stator line current of induction motor, (d) speed of induction motor.

5.3. Transient behavior of SEIG feeding induction motor with PWM based VSI

To start the induction motor successfully, the control algorithm has already been described in the previous section. Figure 8 shows simulation results of the closed-loop performance of the SEIG system with PWM-VSI and P-I controllers. The VSI is connected to the SEIG at t = 1.4 s to synchronize voltage and frequency with the SEIG. The induction motor is connected to the SEIG at t = 1.8 s with no mechanical load, and the induction motor attains the rated speed after the successful starting. The motor electromagnetic torque is also showing appreciable starting transients, which are settled after a few cycles. At t = 2.6 s, full mechanical load (4.5 Nm) is applied to the induction motor. Speed of the induction motor decreases to 273 rad/s and electromagnetic torque increases to 4.5 Nm. At t = 3.3 s, the mechanical load of the induction motor is removed. It is observed that the induction motor attains the rated speed and the electromagnetic torque reaches zero. At t = 3.7 s the speed of the wind changes from 9 m/s to 8 m/s and at t = 4.2 s the speed of the wind change from 8 m/s to 9.5 m/s. As a result, the speed of the SEIG decreases at 3.7 s and the speed of the SEIG increases at t = 4.2 s, but voltage and frequency are maintained constant (415 V r.m.s. and 50 Hz, respectively) by changing the modulation index of the VSI with the help of the PI controller.

5.4. Harmonic analysis of SEIG-fed induction motor with PWM-based VSI

The performance of the SEIG-fed induction motor with PWM-based VSI can be assessed through harmonic analysis and total harmonic distortion (THD) of voltages and currents at generator and load side. The SEIG stator voltage and current waveforms under steady state along with their harmonic spectrum are shown in Figure 9. It has been observed that the THD of the SEIG stator line voltage and currents is 0.09% and 0.19 %, respectively. The THD value of these ranges is well below the limit of 5 % provided in the standard IEEE519.

The experimental setup has been also developed using a TMS320F2812 DSP processor to verify the control technique used and for gate signal generations. This DSP processor has 12-bit, 16 ADC input channels with an input range of 0 to 3 V. The Hall effect voltage sensors are used to sense the actual voltage of the

SEIG, give feedback to the processor through the ADC section of processor, and calculate the peak voltage of the SEIG and then feed it to one input of the PI controller for maintaining the rated SEIG voltage. The second input of the PI controller is the rated SEIG voltage. The PI controller is implemented using a 2812 DSP

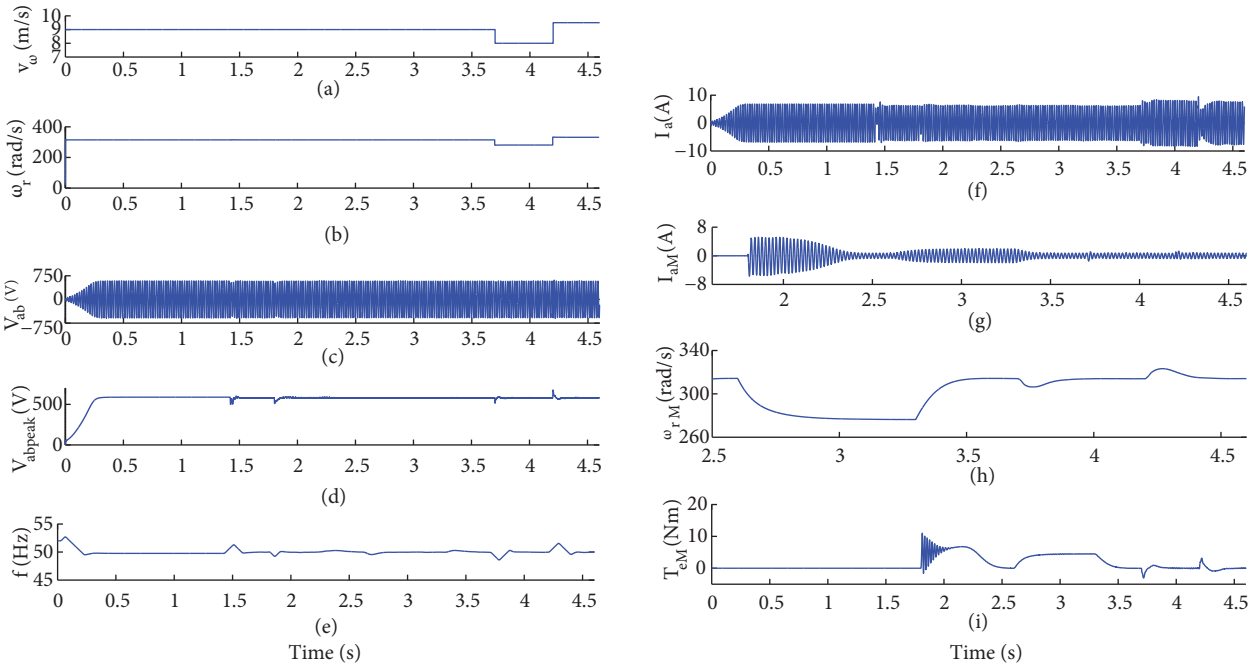

Figure 8. Simulation results of closed-loop SEIG with PWM VSI feeding induction motor: (a) wind speed, (b) rotor speed of SEIG, (c) stator line voltage of SEIG, (d) stator line peak voltage of SEIG, (e) stator frequency of SEIG, (f) stator line current of SEIG, (g) stator line current of induction motor, (h) rotor speed of induction motor, (i) electromagnetic torque of induction motor.

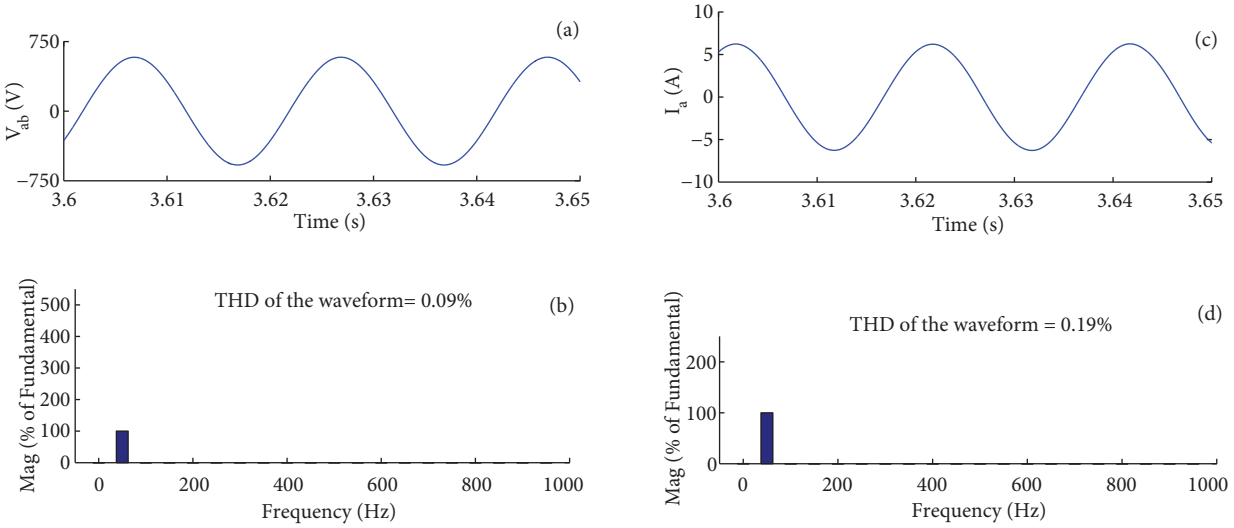

Figure 9. Wave form and harmonic analysis of closed-loop SEIG-fed induction motor: (a) stator line voltage of SEIG, (b) harmonic spectrum of stator line voltage of SEIG, (c) stator line current of SEIG, (d) harmonic spectrum of stator line current.

processor. Depending upon the load and source variations, the PI controller maintains voltage. A switching frequency of 10 kHz is taken for generating gate pulses of a three-leg VSI. Figure 10a shows the gate pulses of two switches of the same leg of the VSI, generated using a TMS320F2812 DSP processor with a dead time of 6 μs for protection. Figure 10b shows the AC line-line output voltage of the PWM VSI. The peak of SEIG phase voltage is calculated (top) using the processor from the sensed SEIG phase voltage (bottom) as shown in Figure 10c.

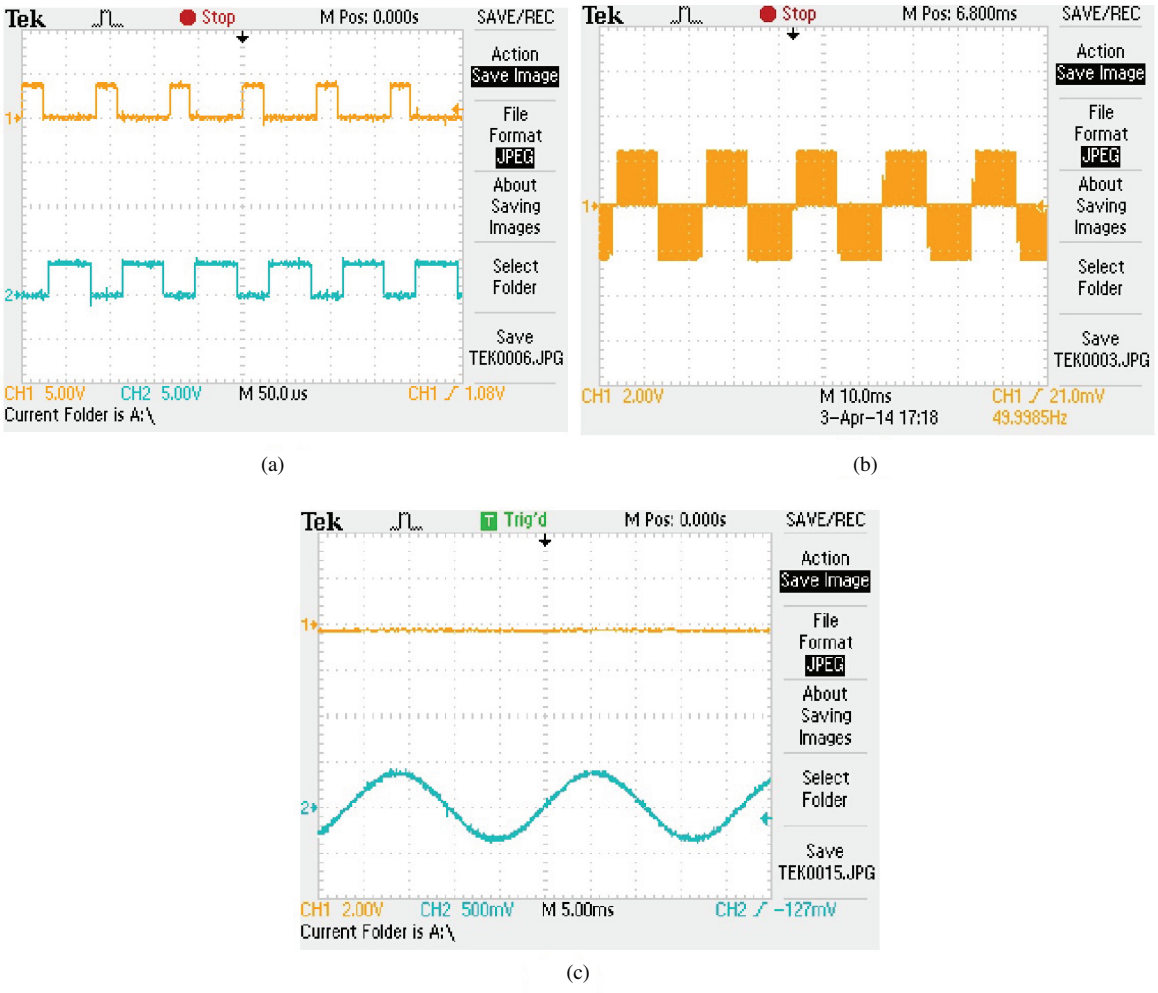

Figure 10. Experimental results of closed-loop control using TMS320F2812 DSP processor: (a) IGBT gate drive pulses of one leg, (b) line-line AC output voltage of VSI, (c) calculated peak of SEIG phase voltage (top) and sensed SEIG phase voltage (bottom).

6. Conclusion

In this paper, the modeling and simulation of a self-excited induction generator with VSI have been carried out to stabilize the system with dynamic load. The transient performance of the self-excited induction generator feeding an induction motor load directly without any control scheme has been compared with those when a PWM VSI is connected at the PCC across the self-excited induction generator and induction motor. It has been observed that the SEIG without any compensator fails to start the induction motor due to sudden collapse

of voltage and current of the SEIG. When the induction motor is connected to a variable-speed wind-driven self-excited generator with PWM VSI, voltage and frequency are regulated because it injects the active power and reactive power demanded by the system. When the prime mover (wind turbine) input increases, the VSI increases active power output from the system to maintain the rated frequency. When prime mover speed decreases, it injects active power to the system to maintain the rated frequency. Similarly, it is also taking care of the reactive power to maintain the rated voltage. The SEIG with the employed control scheme is suitable for a standalone fixed or variable-speed wind-turbine installation for isolated areas feeding the induction motor load. A very low THD value, below 0.2 %, has been obtained with the proposed closed-loop control scheme, which depicts the good power quality. It can be concluded that the proposed controller for the induction motor is satisfactory under steady-state as well as dynamic conditions.

Appendix

The parameters of the wind turbine:

Number of blades	3
Radius of blade	4 m
Rated wind speed	9 m/s
Gear box ratio	5

The parameters of the induction machines used as SEIG and dynamic load are as follows:

Parameters of SEIG: 3.7 kW, 415 V, 7.5 A (line), 50 Hz, 1500 r/min, four poles, delta connected,

$R_s = 7.34\ \Omega,\ R_r = 5.64\ \Omega,\ X_{ls} = 6.7\ \Omega,\ X_{lr} = 6.7\ \Omega$, and $J = 0.16$ kg/m^2.

The constants of the magnetization characteristics of the SEIG are given as:

$a_5 = -0.0038,\ a_4 = 0.0576,\ a_3 = -0.304,\ a_2 = 0.713,\ a_1 = -0.853$, and $a_0 = 1.043$.

Parameters of the induction machine used as dynamic load: 1.5 kW, 415 V, 3.2 A (line), 50 Hz, 1500 r/min, four poles, delta connected,

$R_sm = 0.0832\ pu,\ R_rm = 0.0853\ pu,\ X_{ls} = 0.1101\ pu,\ X_{lr} = 0.1101\ pu,\ X_{mM} = 1.83\ pu$, and $J = 0.0205$ kg/m^2.

Modal matrices of the induction motor are as follows:

$[v_M] = [v_{dsm} \quad v_{qsm} \quad v_{drm} \quad v_{qrm}]^T$

$[i_M] = [i_{dsm} \quad i_{qsm} \quad i_{drm} \quad i_{qrm}]^T$

$[R_M] = diag[R_{sm} \quad R_{sm} \quad R_{rm} \quad R_{rm}]$

$$[L_m] = \begin{bmatrix} L_{lsM} + L_{mM} & 0 & L_{mM} & 0 \\ 0 & L_{lsM} + L_{mM} & 0 & L_{mM} \\ L_{mM} & 0 & L_{lrM} + L_{mM} & 0 \\ 0 & L_{mM} & 0 & L_{lrM} + L_{mM} \end{bmatrix}$$

$$[G_m] = \begin{bmatrix} 0 & 0 & 0 & 0 \\ 0 & 0 & 0 & 0 \\ 0 & -L_{mM} & 0 & -L_{lrM} + L_{mM} \\ L_{mM} & 0 & L_{lrM} + L_{mM} & 0 \end{bmatrix}$$

Nomenclature

ρ	Specific density of air in kg/m^3
r	Radius of wind turbine in m
πr^2	Swept area of the blades
C_P	Performance coefficient of the wind turbine
v_ω	Wind velocity in m/s
ω_T	Rotational speed of wind turbine
$\omega_T r$	Linear speed at the tip of the blade of the turbine
d and q	Direct and quadrature axes
s and r	Stator and rotor variables, respectively
l	Leakage component
v and i	Instantaneous voltage and current, respectively
i_m and L_m	Magnetizing current and magnetizing inductance, respectively
r and L	Resistance and inductance
ω_r	Electrical rotor speed of SEIG
T_{drive} and T_e	Mechanical input torque and electromagnetic torque of the SEIG, respectively
J and P	Moment of inertia and number of poles of generator, respectively
i_{ed} and i_{eq}	Current through the excitation capacitor in d and q axes, respectively
C_{ed} and C_{eq}	Excitation capacitor values in d and q axes, respectively
v_m	Output voltage of SEIG
T_L	Load torque of induction motor
T_{eM}	Electromagnetic torque of induction motor
J_M	Moment of inertia of induction motor
P_M	Number of poles of induction motor
ω_{rM}	Electrical speed of the induction motor

References

[1] Bansal RC, Bhatti TS, Kothari DP. A bibliographical survey on induction generators for application of non - conventional energy systems. IEEE T Energy Conver 2003; 18: 433–439.

[2] Rahim AH, Alam MA, Kadlawala MF. Dynamic performance improvement of an isolated wind turbine induction generator. Comput Electr Eng 2009; 35: 594–607.

[3] Seyoum D, Grantham C, Rahman MF. The dynamic characteristics of an isolated generator driven by a wind turbine. IEEE T Ind Appl 2003; 39: 936–944.

[4] Murthy SS, Malik OP, Tandon AK. Analysis of self-excited induction generators. IEE Proc-C 1982; 129: 260–265.

[5] Lopes LAC, Almedia RG. Wind driven self-excited induction generator with voltage and frequency regulated by a reduced rating voltage source inverter. IEEE T Energy Conver 2006; 21: 297–304.

[6] Geng H, Xu D, Wuare B. Direct voltage control for a stand-alone wind-driven self-excited induction generator with improved power quality. IEEE T Power Electr 2011; 26: 632–641.

[7] Kassem AM. Robust voltage control of a stand alone wind energy conversion system based on functional mode predictive approach. Int J Elec Power 2012; 41: 124–132.

[8] Deraz SA, Kader FEA. A new control strategy for a stand-alone self-excited induction generator driven by a variable speed wind turbine. Renew Energ 2013; 51: 263–273.

[9] Palwalia DK, Singh SP. Digital signal processor based fuzzy voltage and frequency regulator for self-excited induction generator. Electr Pow Comp Sys 2010; 38: 309–324.

[10] Pucci M, Cirrincione M, Lee H. Neural MPPT control of wind generators with induction machines without speed sensors. IEEE T Ind Electron 2011; 58: 37–47.

[11] Wang L, Lee CH. Long shunt and short shunt connections on dynamic performance of a SEIG feeding an induction motor load. IEEE T Energy Conver 2000; 15: 602–608.

[12] Singh SP, Jain SK, Sharma J. Voltage regulation optimization of compensated self-excited induction generator with dynamic load. IEEE T Energy Conver 2004; 19: 724–732.

[13] Singh B, Singh M. Transient performance of series compensated three phase self excited induction generator feeding dynamic loads. IEEE T Energy Conver 2010; 46: 1271–1280.

[14] Chauhan YK, Jain SK, Singh B. Operating performance of static series compensated three-phase self-excited induction generator. Int J Elec Power 2013; 49: 137–148.

[15] Perumal BV, Chatterjee JK. Voltage and frequency control of a standalone brushless wind electric generation using generalized impedance controller. IEEE T Energy Conver 2008; 23: 622–640.

[16] Krause PC. Analysis of Electric Machinery. New York, NY, USA: McGraw Hill, 1987.

[17] Idjdarene K, Rekioua D, Rekioua T, Tounzi A. Performance of an isolated induction generator under unbalanced loads. IEEE T Energy Conver 2010; 25: 303–311.

[18] Dalei J, Mohanty KB. A novel method to determine minimum capacitance of the self-excited induction generator. In: IEEE Tech Symposium; 28 February– 2 March 2014; Kharagpur, India; pp. 408–413.

[19] Jain SK, Sharma JD, Singh SP. Transient performance of three-phase self excited induction generator during balanced and unbalanced faults. IEE Proc-C 2002; 149: 50–57.